Journal of *Marine Science and Engineering*

MDPI

Article

Use of Nanosilica for Increasing Dune Erosion Resistance during a Sea Storm

Elisa Leone [1,*], Nobuhisa Kobayashi [2], Antonio Francone [3], Samuele De Bartolo [1], Davide Strafella [1], Felice D'Alessandro [4] and Giuseppe Roberto Tomasicchio [1]

[1] Department of Engineering for Innovation, University of Salento, EUMER Campus Ecotekne, Via Monteroni, 73100 Lecce, Italy; samuele.debartolo@unisalento.it (S.D.B.); davide.strafella@unisalento.it (D.S.); roberto.tomasicchio@unisalento.it (G.R.T.)
[2] Center for Applied Coastal Research, University of Delaware, Newark, DE 19716, USA; nk@udel.edu
[3] Department of Civil, Environmental, Land, Construction and Chemistry (DICATECh), Polytechnic of Bari, Via Orabona 4, 70125 Bari, Italy; antonio.francone@poliba.it
[4] Department of Environmental Science and Policy, University of Milan, Via Celoria 2, 20133 Milano, Italy; felice.dalessandro@unimi.it
* Correspondence: elisa.leone@unisalento.it

Abstract: Dune recovery interventions that integrate natural, sustainable, and soft solutions have become increasingly popular in coastal communities. In the present study, the reliability of an innovative non-toxic colloidal silica-based solution for coastal sand dunes has been verified for the first time by means of laboratory experiments. An extensive experimental campaign aimed at studying the effectiveness of the use of nanosilica has been conducted in the 2D wave flume of the EUMER laboratory at the University of Salento (Italy). The study was first based on a horizontal seabed and then a cross-shore beach-dune profile was drawn similar to those generally observed in nature. Detailed measurements of wave characteristics and observed bed and cross-shore beach-dune profiles were analyzed for a wide range of wave conditions. In both cases, two sets of experiments were carried out. After the first set of experiments performed resembling the native conditions of the models composed with natural sand, the effects of the injection of the mineral colloidal silica-based grout were investigated. The observations show that mineral colloidal silica increases the mechanical strength of non-cohesive sediments reducing the volume of dune erosion, thus improving the resistance and longevity of the beach-dune system.

Keywords: erosion; vulnerability; eco-recovery; colloidal nanosilica; sediment transport; laboratory experiments; longevity; resistance

check for updates

Citation: Leone, E.; Kobayashi, N.; Francone, A.; De Bartolo, S.; Strafella, D.; D'Alessandro, F.; Tomasicchio, G.R. Use of Nanosilica for Increasing Dune Erosion Resistance during a Sea Storm. *J. Mar. Sci. Eng.* **2021**, *9*, 620. https://doi.org/10.3390/jmse9060620

Academic Editor: Patrick Hesp

Received: 7 May 2021
Accepted: 31 May 2021
Published: 3 June 2021

Publisher's Note: MDPI stays neutral with regard to jurisdictional claims in published maps and institutional affiliations.

Copyright: © 2021 by the authors. Licensee MDPI, Basel, Switzerland. This article is an open access article distributed under the terms and conditions of the Creative Commons Attribution (CC BY) license (https://creativecommons.org/licenses/by/4.0/).

1. Introduction

The continuously growing human population along the coasts of the world will aggravate the impact of human activities on the coastal environments [1]. Therefore, defensive and restoration activities of coastal areas will become increasingly important [2]. Sandy dunes constitute the natural barrier protecting coastal environments against flooding due to storm surge and wave impacts. The process of defense and restoration consists in preventing degradation and assisting the recovery of an ecosystem that has been damaged or destroyed with respect to its health, integrity, and sustainability [3–5]. In the last decades, several soft and hard engineering solutions dealing with coastal dune erosion prevention have been proposed [6,7]. Despite the results in terms of erosion reduction obtained by the installation of engineering structures, a significant alteration of geomorphological processes is rather unavoidable. To improve traditional construction techniques that used rock, concrete, and steel, new alternative techniques are proposed, using geosynthetic materials for revetments, scour protection, and reclamation [8]. In this regard, planting vegetation and/or constructing plant fences along the backshore was found to be a more

natural solution. Installation of planted vegetation limits the mobility of the sand caused by aeolian forces or wave action [9,10]. Nevertheless, a recurrent issue that is addressed in restoration using plants is counteracting the negative impact of depressed biodiversity and even loss of endemic species [11,12]. Moreover, great care must be taken when dealing with changes in geomorphological processes. The collective movement of solid particles, known as sediment transport, is a complex problem related to flow conditions, the nature of the sediment, and the cohesive forces between particles. Historical overviews of the influence of wave conditions, sediment size, sediment gradation, etc., have been extensively studied, for example, by Jonsson [13], Madsen and Grant [14], Sleath [15], Nielsen [16], Fredsøe and Deigaard [17], Van Rijn [18], Soulsby [19], and cross-shore wave mechanics and sediment transport on beaches has been investigated by Nairn and Southgate [20], Kobayashi and Johnson [21], Dean and Dalrymple [22], Tomasicchio et al. [23,24], D'Alessandro and Tomasicchio [25], D'Alessandro et al. [26], Sancho et al. [27], and Brunone and Tomasicchio [28]. These works show the wave-induced bottom shear stress as an essential parameter for calculation of beach erosion and accretion rate and wave height attenuation.

In the present study, the use of nanosilica for coastal sand dune strengthening has been evaluated in the 2D wave flume of EUMER at Unisalento, Lecce (www.eumer.eu, accessed on 10 September 2019). The method concerns the injection of a colloidal silica-based solution into the sand in order to obtain a consolidated layer and reduce the erosion process due to wave action. Testing the performance of the use of nanosilica included two stages. In the first stage, wave-driven sand transport was measured on a mobile sand bed for a wide range of flow conditions. The bed with natural well-sorted fine sand was compared with the bed with the silica-based consolidating material, which changed the cohesive properties of the sand. Observing the behavior of both the natural and consolidated sand has clarified the relationship between the sand properties and hydrodynamic loadings (e.g., bed shear stress). Thereafter, physical model tests on the morphological development of the beach-dune system under irregular waves were conducted with the aim of observing and comparing the behavior of natural and consolidated sand. The conducted experiments, including setup, data analysis, and comparison of the data are presented in the following sections.

2. Laboratory Facility and Nanosilica Grout

2.1. Experimental Facility

In the framework of the INNODUNE project, physical model tests were conducted in a 2D wave flume at the EUMER lab, Campus Ecotekne, Lecce (Figure 1). The flume is 45 m long, 1.5 m wide, and 2 m deep. The wave generation is performed by a single paddle equipped with an active wave absorption system allowing tests to be run without the effect of spurious model-induced reflections. Froude's law was selected as the proper criterion to down-scale the hydrodynamic parameters; however, on fine-grained sand beaches, the geometric scaling leading to a clay-size sediment were avoided to prevent the inception of cohesive effects [29]. Therefore, the grain size of the sediment in the flume is not scaled by the geometric scale, resulting in the same sand in the model [30]. The sediment is well-sorted fine sand with a median diameter d_{50} of 0.245 mm. The measured density of sediment grains, ρ_s, and porosity, ε, of the sand are 2.6 g/cm^3 and 0.4, respectively. The experimental program involved measurements of time-varying water level and bed profile. A wave gauge system from HR Wallingford acquired the water level with an accuracy of the order of 0.1 mm [31], enabling both statistical and spectral analysis of the waves through the HR DAQ data acquisition and analysis software program.

The cross-shore profile is observed with the laser profiler described by HR Wallingford. The system consists of a vertical position controlled device driven by a small electric motor with a mechanical transmission actuating a rod. At the lower end of the rod, a low-powered laser distance sensor mounted inside a waterproof housing is provided. The position of the probe is measured by encoders on the moto shafts, leading to the observation of the bed height, even rather inclined and irregular profile, with an accuracy of the order of

0.1 mm [32]. The bed profile observation is performed by the horizontal motion of the vertical servo controlled device placed in a carriage.

Figure 1. Top view (**left**) and side view (**right**) of 2D wave flume at EUMER lab, Unisalento.

2.2. Nanosilica-Based Grout

The additive to consolidate the sand consists of a non-toxic aqueous suspension with dispersed nanometric particles of colloidal silica (Figure 2). These particles are made of quartz (SiO_2) with a tetrahedral distribution of the atoms which makes the mixture completely mineral, highly reactive, and more stable than other quartz-based crystalline compounds. Before injecting nanosilica into the sand, an accelerator, i.e., a solution of sodium chloride (10% NaCl in water), is added to the suspension.

Figure 2. Aqueous suspension of colloidal nanosilica.

The solution acts as an activator, triggering a gelification process that induces the suspension to become a gel. Depending on the dosage, the accelerator adjusts the product workability time [33]. Nanosilica, before gelation, has a very low viscosity (very close to water: about 10 mPa·s compared to 1 mPa·s), which means a very high permeation and penetration capacity.

After mixing the components, the dispersion of the nanosilica-based grout was carried out by a pressure pulverizer at 20 °C, penetrating into the surface layer of the sand. After spraying the grout and completion of the gelling time, a homogeneous consolidation of the sand was observed. The result consisted of a pore-filling process and an increase in cohesion of the sand; nevertheless, the nanosilica-based material did not interfere with germination or seedling growth because permeability was ensured. On a control volume, different amounts of nanosilica were tested, defined by a percentage of the grout relative to

the voids in the sand. In particular, tested amounts were 5%, 2%, and 1% which resulted in a consolidated sand layer of different depth, h_c, and porosity ε (Table 1). In Figure 3, samples of consolidated layers are shown.

Table 1. Characteristics of consolidated layers of each percentage of nanosilica.

Percentage of Nanosilica	h_c [cm]	ε [-]
5%	3.0	0.20
2%	1.5	0.24
1%	0.8	0.25

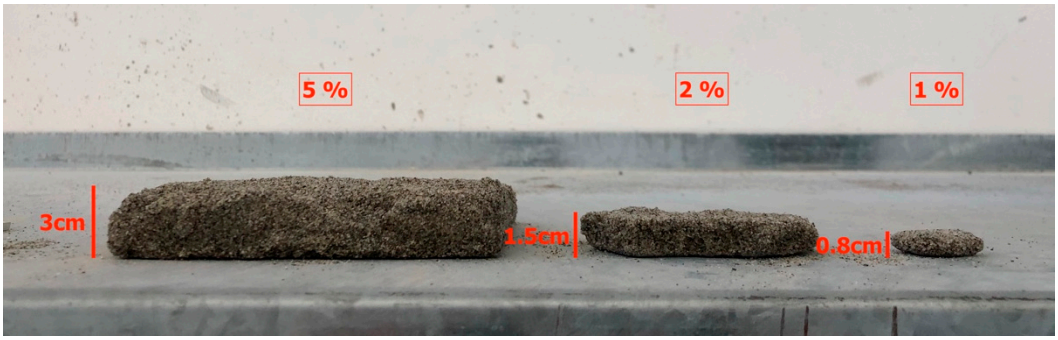

Figure 3. Samples of consolidated layers for different percentages of nanosilica: 5%, 2%, and 1%.

3. Horizontal Bed Experiments

The first part of the experimental campaign was carried out on a horizontal seabed. The experiment was conducted because the wave boundary layer on a horizontal bed is well understood. The bottom shear stress on natural and consolidated sands can be estimated using existing wave boundary layer models. In the wave flume, two concrete blocks with a triangular transversal geometry and 1:3 slope were positioned at a distance of 2 m from each other. The blocks were 0.3 m high, 0.9 m long, and as wide as the width of the flume. The 2-m gap between the blocks was filled with sand. A picture of the first physical model is shown in Figure 4.

Figure 4. Horizontal sand bed layout.

One wave gauge (WG1) was located as close as possible to the wave generator and three wave gauges (WG2–WG4) were used to evaluate the wave conditions over the horizontal seabed and to separate incident and reflected waves in the wave flume. The bed

profile was observed with the laser profiler for an extension of 1.5 m on the seabed to avoid the edge effects due to the slopes. A side view of the full experimental setup is shown in Figure 5.

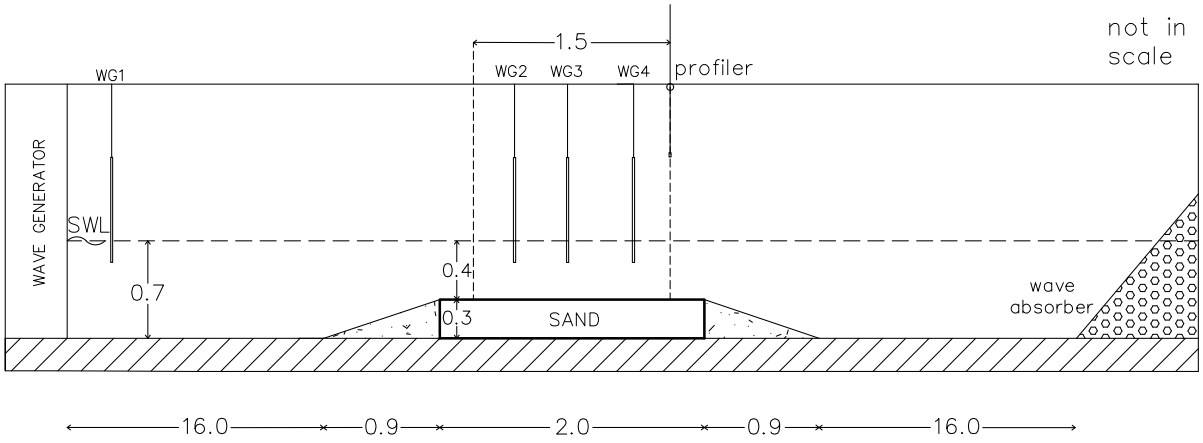

Figure 5. Side view of experimental setup of the horizontal seabed model.

Non-breaking wave conditions were adopted. Regular and irregular wave tests were conducted on the horizontal seabed. The incident and reflected wave parameters were obtained using the theory of Mansard and Funke [34]. The reflection coefficient, k_r, defined as the ratio between the reflected and incident wave height was less than 0.25. Table 2 lists the incident wave characteristics in sequence. In particular, tests marked with HN (Horizontal Natural) refer to a movable bottom of natural sand without adding colloidal nanosilica. Tests marked with HC (Horizontal Consolidated) refer to a condition of sand with a percentage of nanosilica calculated so as to achieve a consolidated sand layer of 5 cm. The regular wave conditions are defined by wave height, H, and wave period, T. The irregular wave conditions are based on a Jonswap spectrum with peak enhancement factor, γ, equal to 3.3, and defined by energy-based significant wave height, H_{m0}, and peak period, T_p. Three water depths above the bed, h, were chosen, starting from 0.4 m increased by 0.1 m up to 0.6 m. The water depth in front of the wave generator was (h + 0.3) m. Two tests of regular waves and two tests of irregular waves were carried out for each h. The duration of wave attacks was defined considering the time required for bed form to develop evenly along the seabed [35]. In particular, for regular waves, a number of waves were specified to be generated; under irregular waves, the bed forms may grow slowly, especially under low velocities that are not much above threshold. Some exploratory experiments were conducted to determine the necessary durations. In both cases, the total duration also includes the time the wave takes to reach the model and return to the wave generator which, for convenience, has been associated with the duration of 30 waves. This calculated time was excluded during wave data analysis [35].

Wave parameters are subject to changes due to wave transformation and wave height may decrease, due to wave energy loss. The intensity of wave energy dissipation depends on the incident wave height, water depth, and bottom characteristics. Using the wave conditions acquired in HC and HN tests, the amplitude of the wave orbital velocity, U_w, and one half of the horizontal orbital excursion, A_w, just above the bottom boundary layer for regular waves were calculated as [19]:

$$U_w = \frac{\pi H}{T \sinh(kh)}$$
$$A_w = \frac{U_w T}{2\pi} \quad (1)$$

where *sinh* is the hyperbolic sine, $k = \frac{2\pi}{L}$ is the wave number, L is the wavelength, and h the water depth over the seabed. For irregular waves, H and T are replaced by H_{m0} and T_p.

Table 2. Incident of regular and irregular wave characteristics on the horizontal seabed.

Test Group	Test Name	Wave Type	h [m]	H/H_{m0} [m]	T/T_p [s]	Duration [s]
HN	HN1	Regular	0.40	0.116	1.00	180
	HN2		0.40	0.138	1.20	216
	HN3		0.50	0.153	1.79	324
	HN4		0.50	0.219	1.99	360
	HN5		0.60	0.195	1.79	324
	HN6		0.60	0.220	2.19	396
	HN7	Irregular	0.40	0.095	1.48	8145
	HN8		0.40	0.118	1.79	2574
	HN9		0.50	0.146	2.01	2460
	HN10		0.50	0.183	2.42	1752
	HN11		0.60	0.182	2.15	1606
	HN12		0.60	0.206	2.41	1752
HC	HC1	Regular	0.40	0.118	1.00	180
	HC2		0.40	0.141	1.20	216
	HC3		0.50	0.160	1.80	324
	HC4		0.50	0.227	2.00	360
	HC5		0.60	0.209	1.80	324
	HC6		0.60	0.231	2.19	396
	HC7	Irregular	0.40	0.097	1.48	8145
	HC8		0.40	0.120	1.80	2574
	HC9		0.50	0.153	2.02	2460
	HC10		0.50	0.189	2.46	1752
	HC11		0.60	0.188	2.15	1606
	HC12		0.60	0.211	2.42	1752

Bed form conditions responded to increasing wave energy for HN2–12. The measured ripple height and wavelength were estimated about 1 cm and 10 cm, respectively. In the remaining tests (HN1 and HC1–12) the seabed configuration did not change in response to the wave attack, remaining flat.

4. Movement of Natural and Consolidated Sands

An estimate of the threshold of motion can be given by the Shields parameter, θ_0, in terms of the ratio of the force exerted by the bed shear stress acting on a grain on the bed, to the submerged weight of the grain counteracting this [19]. The bed shear stress, τ_w, represents the most important hydrodynamic property of waves for sediment transport purposes. It is usually obtained from U_w and the bottom friction factor, f_w. Acting on the bed, τ_w is made up of contributions due to the skin friction, τ_{ws}, produced by (and acting on) the sediment grains and the form drag, τ_{wf}, produced by the pressure field associated with the flow over ripples and/or larger features on the bed. If the bed is flat and sediment transport is not intense, the distinction between total and skin friction quantities is not necessary. It is important to be aware that only the skin friction contribution acts directly on the sediment grains, and the skin friction is normally used to calculate the threshold of motion, bedload transport, and reference concentration or pick-up rate for grains in suspension. On the other hand, it is the total bed shear stress that corresponds to the overall resistance of the flow and determines the turbulence intensities which influence the diffusion of suspended sediment higher in the water column. In literature, several expressions of f_w were found with a great variability in terms of Reynolds number, $Re = \frac{A_w U_w}{\nu}$, where ν is the kinematic viscosity, and the relative roughness, $\frac{A_w}{k_N}$, where k_N is the Nikuradse equivalent bed roughness. k_N can be written as sum of grain-related

k_{Ns} and form drag k_{Nf} components. Among the available formulas, the formulation by Soulsby [19] was adopted to calculate f_w. This is a choice taken by many authors [36–38]. The formulation by Soulsby does not depend on the wave Reynolds number, and a rough turbulent bed is assumed. Therefore, θ_0, τ_w, and f_w are defined by:

$$\theta_0 = \frac{\tau_w}{g\,(\rho_s - \rho) d_{50}}$$
$$\tau_w = \frac{1}{2}\rho f_w U_w{}^2 \quad (2)$$
$$f_w \; depends \; on \; \frac{A_w}{K_N}$$

where g is the acceleration due to gravity, ρ is the density of the water, and the density and the median diameter of the sand are ρ_s =2.6 g/cm^3 and d_{50} =0.245 mm in this study.

In the present work, K_N is evaluated in the form $K_N = 2.5\, d_{50}$ proposed by Nielsen (1992) [16].

According to Shields, the sediment movement may be observed when a critical value of bed shear stress is reached with a typical value of θ_0 is of about 0.05 [39]. Figure 6 shows the calculated θ_0 for each test considering only the skin friction shear stress contribution which acts directly on the sediment grains.

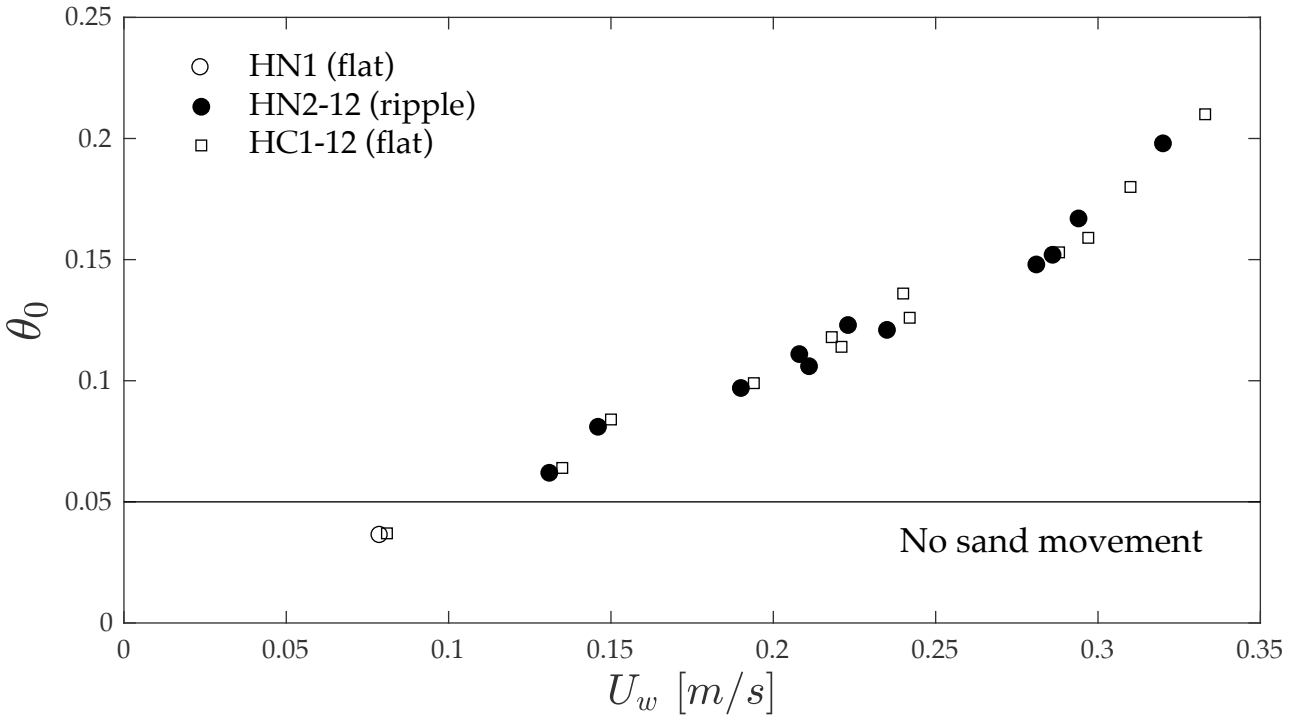

Figure 6. θ_0 for HN and HC test groups as a function of U_w.

In HN tests, the results were consistent with Shield's theory. In tests with θ_0 greater than 0.05, mobilization at the bottom was observed. Only in the case of HN1, the critical value not reached. On the other hand, in HC tests, although the threshold θ_0 is reached, mobility at the bottom was not observed. In particular, the largest value of θ_0 was observed in the HC4 regular wave test with a duration of 360 s corresponding to a consolidated sand resistance force per unit area of 0.81 N/m^2. For irregular waves, θ_0 became as large as 0.16 in the HC10 with a duration of 1752 s, reaching a consolidated sand resistance force per unit area of 0.61 N/m^2.

This experiment indicated the practical utility of nanosilica grout but, since its performance against breaking waves is unknown, new experiments using breaking waves were carried out.

5. Dune Erosion Experiments

A second part of the experimental campaign consisted of a model beach-dune system located at 23.3 m from the wave generator. The model in the flume had a length of 6.9 m. The beach had a slope of 1/10 by an extension of 5.2 m and a slope of 1/50 by an extension of 0.2 m. The dune length was 1.5 m with a seaward slope of 1/1.5. The dune crest length was 0.5 m, and the dune height above the toe was 0.35 m. These slope gradients are typically observed along the Italian coastline. The still water level (SWL) was chosen in such a way that the part of the beach with a slope of 1/10 was mostly submerged and the part with a slope of 1/50 was fully emerged. Waves were measured using wave gauges WG1-WG7. A side view of the beach-dune system as built with the instrumentation is shown in Figure 7. The origin along the onshore coordinate is taken at WG2. WG1 was located as near as possible to the wave generator to check the accuracy of the wave generation and wave absorption capability of the wave maker. The remaining gauges measured the free surface elevations from the offshore and wave shoaling zones and for reflection analysis following the theory of Mansard and Funke [34]. Given the bathymetry, WG2-WG3-WG4 were placed before the beach and WG5-WG6-WG7 before the dune. In Table 3, the onshore coordinate X (m) and water depth below SWL at each of the seven WGs are listed.

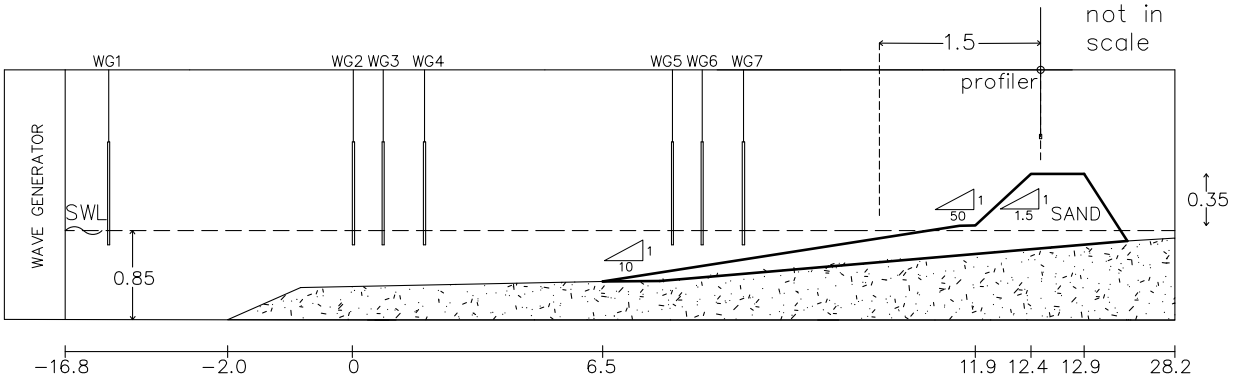

Figure 7. Side view of experimental setup of beach-dune system model.

Table 3. Onshore coordinate X and water depth below SWL at WG1-WG7.

Wave Gauge (WG)	WG1	WG2	WG3	WG4	WG5	WG6	WG7
Onshore X [m]	−15.8	0	0.4	0.9	7.0	7.3	7.7
Depth [m]	0.85	0.53	0.53	0.52	0.44	0.41	0.38

The cross-shore profile of the beach-dune system is measured with the laser profiler in the zone of noticeable profile changes x = 11.0 m–12.5 m (1.5 m onshore distance). This choice stems from the fact that the nanosilica-based grout was sprayed from the toe up to the crest of the dune to evaluate the increase of the erosion resistance exclusively on the dune face.

Two sets of tests were carried out allowing the observation of the dune erosion process and comparison with the behavior of the system with the nanosilica grout. After the first set of tests, performed resembling the native conditions of the beach-dune system made of natural well-sorted fine sand, the effects of spraying the colloidal silica-based grout over the face of the dune were investigated. Seven dune tests (D) using natural (N) and consolidated (C) sands were carried out. The wave conditions are defined by H_{m0} and T_p at WG 2–4 outside the surf zone and the wave steepness $s = \frac{2\pi}{g}\frac{H_{m0}}{T_p^2}$ is between 0.01

and 0.07. Starting from time t = 0, the initial profile was exposed to four runs composed of 230, 230, 330, and 330 waves, respectively. The beach profile was measured after each run [35]. Again, 30 waves were excluded during wave data analysis for each run. Table 4 summarizes the incident wave characteristics in the dune erosion experiments.

Reflection coefficients appear relatively large because of the steep dune slope, typically observed along the Italian coastlines and exposed to waves that are not too large. Table 4 shows similar wave characteristics for the corresponding test, DNj and DCj, with j = 1–7. The differences are less than 10% for H_{m0}, 15% for T_p, and 20% for k_r.

Table 4. Incident irregular wave H_{m0}, T_p, $s = \frac{H_{m0}}{\left(gT_p^2/2\pi\right)}$, and reflection coefficient k_r at WG 2–4.

Test	Run	H_{m0} [m]	T_p [s]	s [-]	k_r [-]	Test	Run	H_{m0} [m]	T_p [s]	s [-]	k_r [-]
DN1	1	0.101	1.17	0.047	0.203	DC1	1	0.104	1.17	0.048	0.189
	2	0.104	1.14	0.051	0.199		2	0.104	1.20	0.047	0.207
	3	0.098	1.19	0.044	0.198		3	0.100	1.19	0.045	0.217
	4	0.097	1.19	0.044	0.188		4	0.100	1.19	0.045	0.227
DN2	1	0.116	1.56	0.030	0.257	DC2	1	0.116	1.56	0.031	0.253
	2	0.115	1.56	0.030	0.236		2	0.116	1.56	0.031	0.260
	3	0.114	1.57	0.030	0.235		3	0.114	1.57	0.030	0.272
	4	0.114	1.54	0.031	0.235		4	0.114	1.53	0.031	0.280
DN3	1	0.118	1.99	0.019	0.299	DC3	1	0.121	1.99	0.020	0.337
	2	0.118	1.99	0.019	0.279		2	0.121	2.02	0.019	0.344
	3	0.117	2.16	0.016	0.258		3	0.120	2.21	0.016	0.321
	4	0.117	2.27	0.015	0.238		4	0.120	2.21	0.016	0.325
DN4	1	0.123	2.49	0.013	0.402	DC4	1	0.124	2.42	0.014	0.388
	2	0.123	2.45	0.013	0.401		2	0.123	2.42	0.013	0.397
	3	0.122	2.55	0.012	0.379		3	0.122	2.47	0.013	0.386
	4	0.122	2.53	0.012	0.363		4	0.122	2.47	0.013	0.386
DN5	1	0.155	1.23	0.065	0.256	DC5	1	0.152	1.23	0.064	0.259
	2	0.154	1.23	0.065	0.269		2	0.152	1.23	0.064	0.265
	3	0.150	1.19	0.068	0.247		3	0.149	1.19	0.068	0.267
	4	0.151	1.19	0.068	0.254		4	0.146	1.19	0.066	0.251
DN6	1	0.188	1.52	0.052	0.299	DC6	1	0.202	1.53	0.055	0.283
	2	0.188	1.52	0.052	0.294		2	0.202	1.53	0.055	0.295
	3	0.184	1.52	0.051	0.289		3	0.196	1.54	0.053	0.305
	4	0.183	1.54	0.049	0.284		4	0.195	1.56	0.051	0.312
DN7	1	0.188	1.99	0.030	0.259	DC7	1	0.208	1.99	0.034	0.278
	2	0.188	1.99	0.030	0.267		2	0.208	1.99	0.034	0.294
	3	0.185	2.27	0.023	0.235		3	0.208	1.99	0.034	0.297
	4	0.185	2.27	0.023	0.231		4	0.199	1.99	0.032	0.244

6. Erosion of Natural and Consolidated Dunes

In the beach-dune model, incident wave characteristics observed between the offshore and shoaling zones were analyzed to examine the cross-shore wave transformation. In the DN and DC tests, H_{m0}, T_p, and k_r at WG 2–4 and WG 5–7 were compared and shown in Figure 8 for all the tests with the four runs.

In most of the tests, the wave showed no significant change from WG 2–4 to WG 5–7, except for the DN6-DC6 and DN7-DC7 in which H_{m0} decreased due to wave breaking. Comparing the results between the DN and DC tests, k_r increased along the flume in the cases of consolidated sand. The above tendencies are associated with the application of nanosilica to the dune, which limits the erosion of the steep dune face. This behavior is most evident in test DC7, where k_r increased from about 0.28 at WG 2–4 to about 0.36 at WG 5–7 because of the decrease of H_{m0} due to wave breaking.

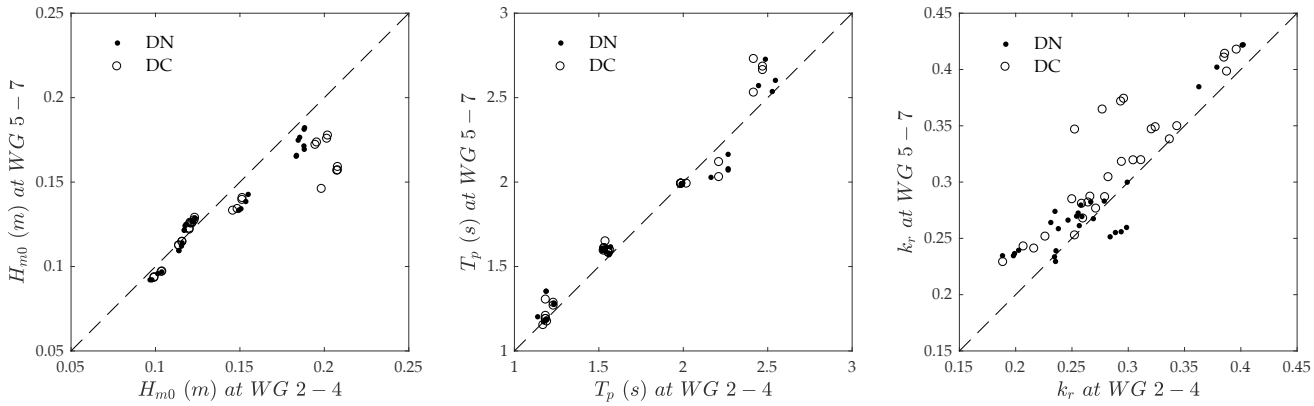

Figure 8. Comparison of wave characteristics of WG 2–4 and W G5–7 for DN and DC tests.

The erosion process of the beach-dune system was observed. Before each new test, the initial conditions of the beach-dune system were restored. It is important to note that it is difficult to exactly reconstruct the same model geometry at the start of each test. Although some geometric parameters were unidentical for all tests (e.g., dune height), the deviation is small enough that they can be considered constant. The process of dune face erosion in the DN tests changed as the test continued. Initially, the slope of the dune face was 1/1.5 (vertical/horizontal). Many waves reach and erode the dune face. The scarped dune front becomes steeper until it is nearly vertical. Then, after a first series of waves within the first run, a different erosion mechanism starts. The dune face only retreats under waves impacting it. Episodically, the dune face collapses and big lumps of sediment fall or slide down the dune face on the beach in front of the dune. This sand is picked up by swash and inner surf zone processes that move the sediment further seaward extending the new foreshore. At this stage of the erosion process, the number of waves impacting the dune is certainly lower, consequently the erosion rate is reduced. In the DC tests, the injection of the nanosilica protected the surface layer of the dune exposed to run up, so the erosion process did not take place in the first series of waves, as in the DN tests. The dune face remained unchanged for a higher number of waves. A front and side view of the cross-shore profile after four runs of DN4 and DC4 is shown in Figure 9 in order to appreciate the effect of nanosilica on the dune face.

The cross-shore profiles of the beach-dune system were evaluated by the laser profiler attached to a mobile platform with x-axis defined positively onshore from x = 11 m up to x = 12.5 m (see Figure 7). Before the start of each test as well as after every wave run, profiles were recorded along the centerline. The profiler velocity was set in order to have a horizontal resolution of 0.2 mm. Figure 10 presents the comparison of the observed cross-shore profiles of DN4 and DC4.

For the DN4 test, a progressive erosion of the dune face from the first run up to the end of the test was observed. An offshore transport was noticeable from the crest, leading to sand being deposited on the toe of the dune and onto the underlying beach. This is compounded by onshore sand transport increasing sand accumulation at the toe area. Focusing on the DC4 test, it is evident that the cross-shore profile of the dune face did not changed as a result of the injection of the nano-silica based grout. Only the onshore transport was observed, leading to accumulation (of a lower magnitude than DN4) at the toe of the dune and erosion in the inner surf zone.

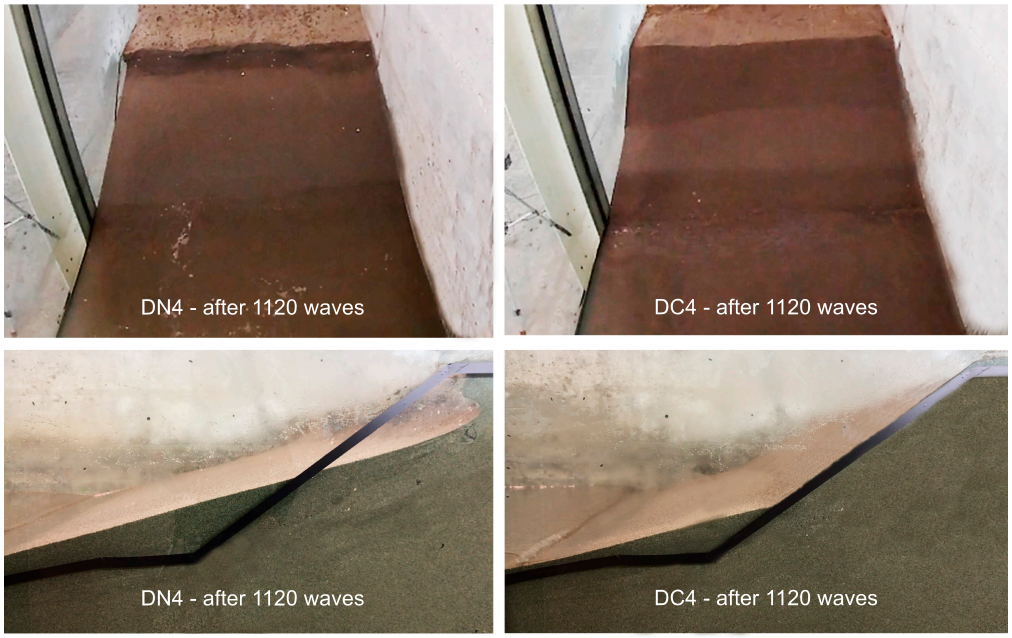

Figure 9. Front view (**up**) and side view (**down**) of cross-shore profile after four runs of DN4 and DC4.

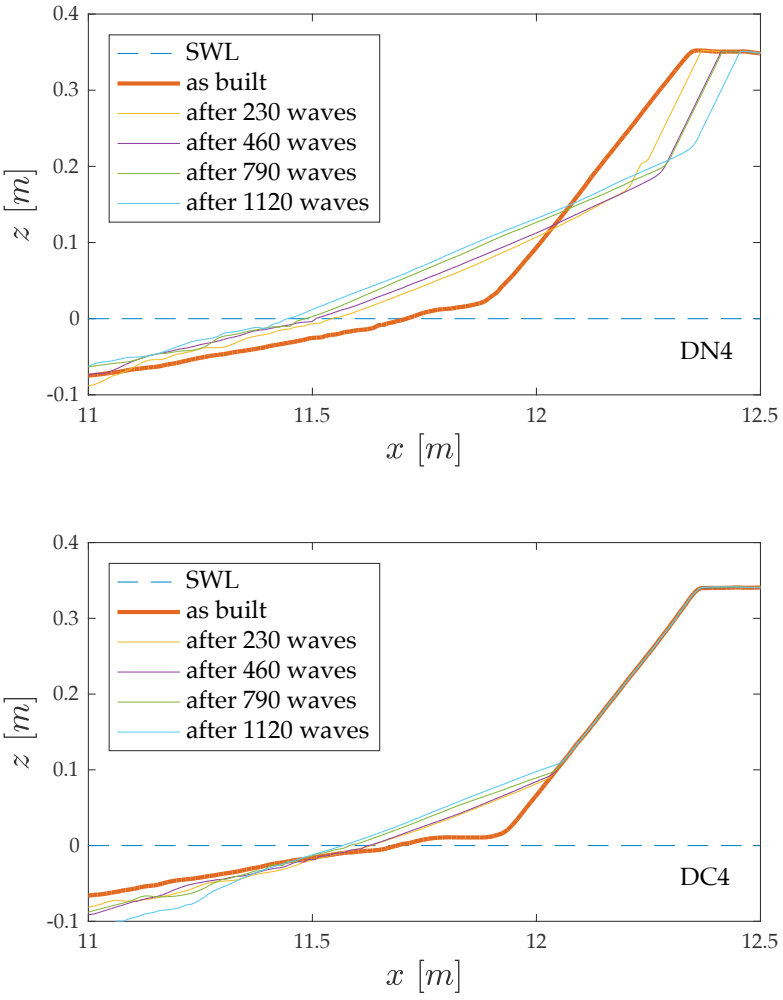

Figure 10. Measured cross-shore profiles after 230, 460, 790, and 1120 waves for tests DN4 (**up**) and DC4 (**down**).

Erosion progression of the dune was analyzed in order to quantify the effect of the nanosilica-based grout on the dune surface. The eroded area, A_e, after each run of the DN and DC tests was normalized by the square of H_{m0} observed at WG 2–4. Table 5 lists the sequence of the normalized area $A_* = \frac{A_e}{H_{m0}^2}$ and the wave steepness s based on H_{m0} and T_p at WG 2–4 for the DN and DC tests.

Figure 11 shows A_* as a function of s for tests DN1-DN7 for increasing number of waves. Empirical formula for dune erosion can be found for $s = 0.012 - 0.068$ by fitting an exponential function of the observed data for each number of waves as:

$$A_{*,n} = a(N)\, e^{-b(N)*s} \tag{3}$$

where the subscript n indicates that the formula is valid for tests with natural sand, N is the number of waves from 230 to 1120, and a and b are the exponential function coefficients listed in Table 6.

Table 5. Wave steepness $s = \frac{H_{m0}}{(gT_p^2/2\pi)}$ at WG 2–4 and measured A_e and $A_* = \frac{A_e}{H_{m0}^2}$ for DN and DC tests.

Test	Run	s [-]	A_e [m^2]	A_* [-]	test	Run	s [-]	A_e [m^2]	A_* [-]
DN1	1	0.047	0.0018	0.175	DC1	1	0.048	0.0001	0.009
	2	0.051	0.0019	0.177		2	0.047	0.0001	0.009
	3	0.044	0.0020	0.209		3	0.045	0.0001	0.010
	4	0.044	0.0022	0.235		4	0.045	0.0002	0.020
DN2	1	0.030	0.0045	0.336	DC2	1	0.031	0.0001	0.007
	2	0.030	0.0059	0.443		2	0.031	0.0001	0.007
	3	0.030	0.0081	0.625		3	0.030	0.0002	0.015
	4	0.031	0.0087	0.671		4	0.031	0.0002	0.015
DN3	1	0.019	0.0032	0.229	DC3	1	0.020	0.0001	0.007
	2	0.019	0.0049	0.355		2	0.019	0.0002	0.014
	3	0.016	0.0050	0.365		3	0.016	0.0002	0.014
	4	0.015	0.0068	0.497		4	0.016	0.0004	0.028
DN4	1	0.013	0.0150	0.985	DC4	1	0.014	0.0001	0.007
	2	0.013	0.0208	1.370		2	0.013	0.0001	0.007
	3	0.012	0.0227	1.525		3	0.013	0.0001	0.007
	4	0.012	0.0247	1.673		4	0.013	0.0002	0.013
DN5	1	0.065	0.0026	0.108	DC5	1	0.064	0.0001	0.003
	2	0.065	0.0035	0.149		2	0.064	0.0001	0.004
	3	0.068	0.0037	0.166		3	0.068	0.0002	0.009
	4	0.068	0.0047	0.207		4	0.066	0.0002	0.009
DN6	1	0.052	0.0049	0.139	DC6	1	0.055	0.0001	0.002
	2	0.052	0.0069	0.195		2	0.055	0.0002	0.005
	3	0.051	0.0101	0.300		3	0.053	0.0002	0.005
	4	0.049	0.0152	0.452		4	0.051	0.0101	0.265
DN7	1	0.030	0.0116	0.327	DC7	1	0.034	0.0001	0.002
	2	0.030	0.0121	0.342		2	0.034	0.0001	0.002
	3	0.023	0.0186	0.541		3	0.034	0.0001	0.002
	4	0.023	0.0227	0.667		4	0.032	0.0123	0.312

Based on the analysis of the test results, the effect of T_p on dune erosion in terms of A_* was evident. In particular, A_* was larger for lower values of s, confirming its dependency on T_p in accordance with van Gent et al. [40].

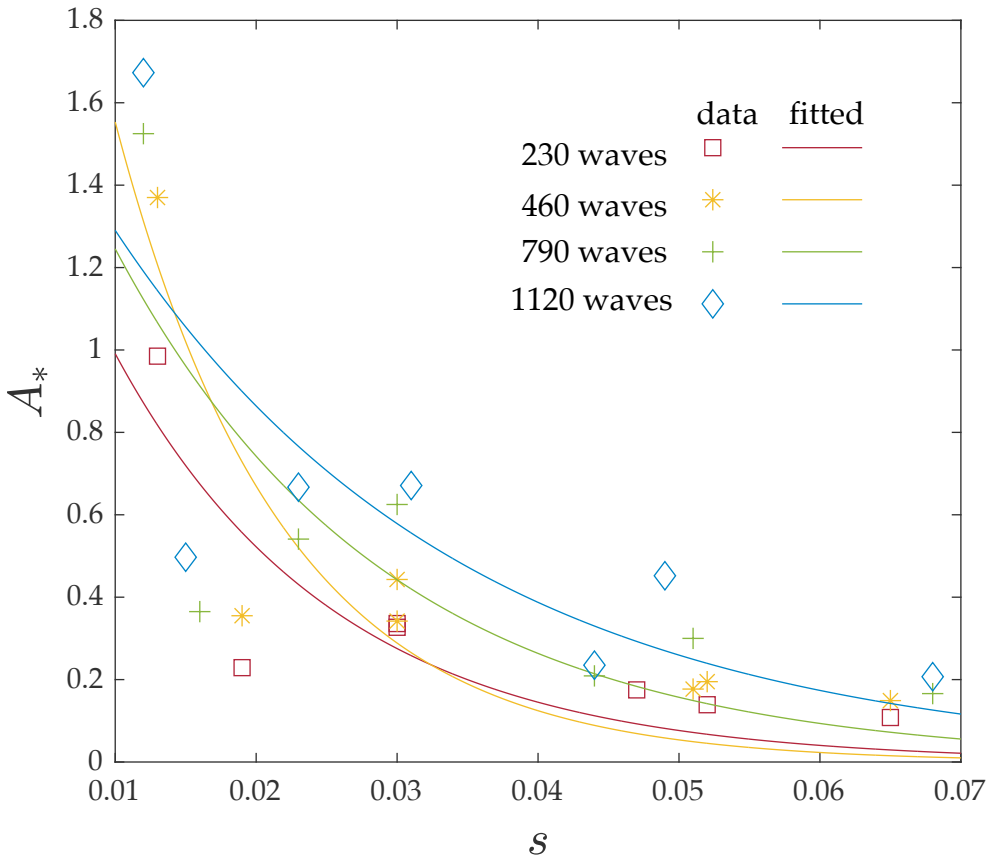

Figure 11. Normalized eroded area A_* after 230, 460, 790, and 1120 waves as a function of wave steepness s for tests DN1-DN7.

Table 6. a and b as a function of N for tests DN1-DN7.

N	a	b
230	1.88	64.0
460	3.60	84.1
790	2.09	51.8
1120	1.93	40.1

For tests DC1-DC7, a significant reduction in A_* was observed. The erosion threshold, in terms of A_*, is 0.05 except for DC6 and DC7, which exhibited a higher value for N = 1120. Figure 12 shows A_* as a function of s in the DN and DC tests for increasing N. The difference in terms of A_* between the DN and DC tests is significant because the erosion in the DC tests was significantly reduced; nevertheless, erosion was observed at DC6 and DC7, between waves 790 and 1120. The present experiments suggest the limitations of the nanosilica grout in terms of erosion resistance and durability because of the fairly sudden failure of the nanosilica grout.

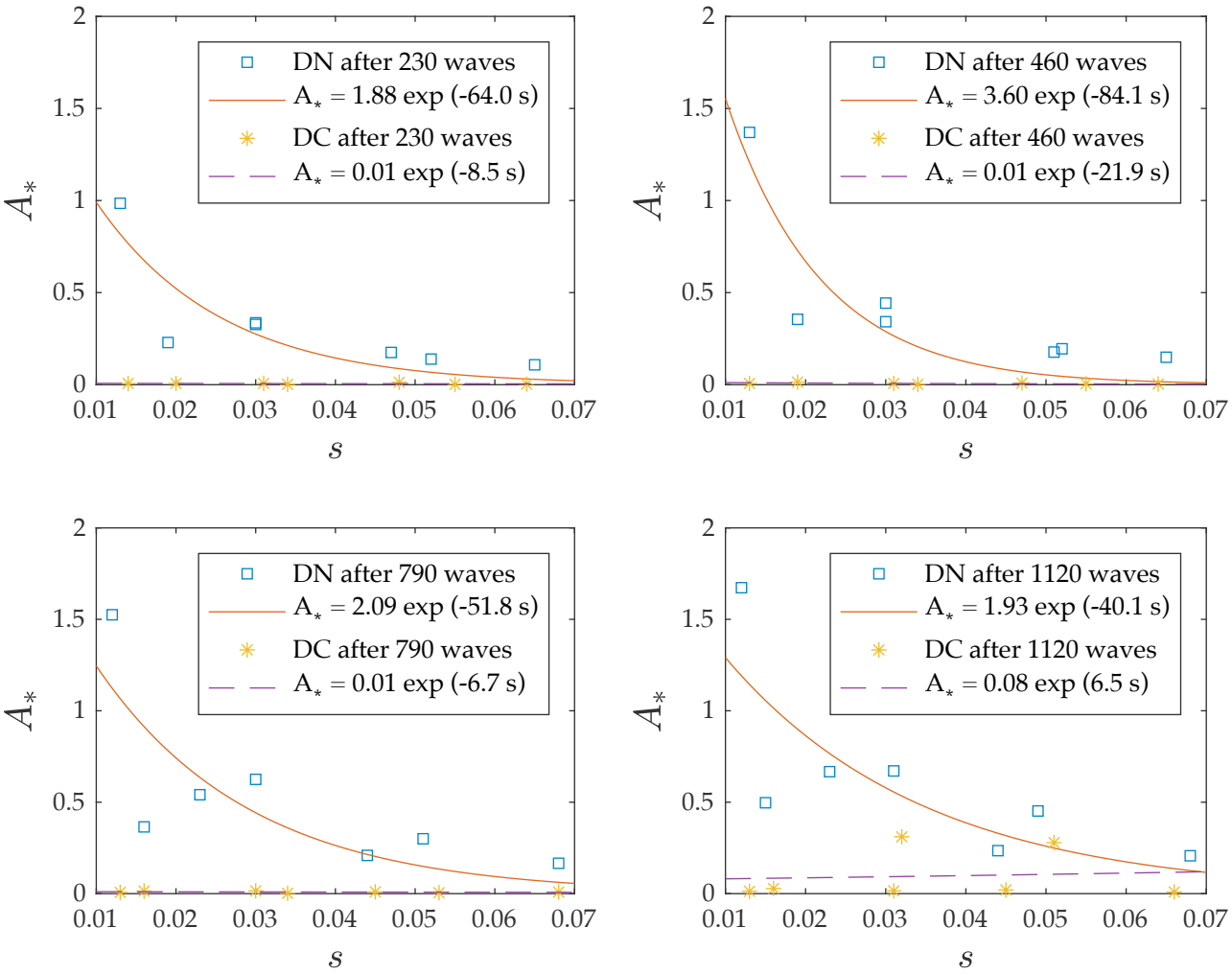

Figure 12. A_* as a function of s in the DN and DC tests for N = 230 (**upper left**), 460 (**upper right**), 790 (**lower left**), and 1120 (**lower right**).

The general empirical formula, for both DN and DC tests, is expressed as:

$$A_* = R\, a(N)\, e^{-b(N)*s} \tag{4}$$

where R is defined as the reduction factor for the consolidated sand:

$$\begin{aligned} R &= 1 \qquad \text{For natural sand} \\ R &= \frac{A_*}{a\, e^{(-b\, s)}} \quad \text{For consolidated sand} \end{aligned} \tag{5}$$

Equation (5) implies that $R < 1$ in the DC tests accounts for the effect of increased erosion resistance. The estimated $a\, e^{(-b\, s)}$ using Table 6 and R using A_* in DC tests are listed in Table 7. A significant reduction in erosion was confirmed, with a threshold in terms of R, of 0.28 except for DC6 and DC7 for the number of waves equal to 1120. The reduction factor of R will need to be predicted for actual field applications of the nanosilica grout.

Table 7. Wave characteristics for DC tests, estimated $a\ e^{(-b\ s)}$ for DN tests and R for DC tests.

Test	H_{m0} [m]	T_p [s]	s [-]	N	ae^{-bs}	R
DC1	0.104	1.17	0.048	230	0.09	0.10
	0.104	1.20	0.047	460	0.05	0.19
	0.100	1.19	0.045	790	0.21	0.05
	0.100	1.19	0.045	1120	0.33	0.06
DC2	0.116	1.56	0.031	230	0.27	0.03
	0.116	1.56	0.031	460	0.28	0.03
	0.114	1.57	0.030	790	0.45	0.03
	0.114	1.53	0.031	1120	0.56	0.03
DC3	0.121	1.99	0.020	230	0.55	0.01
	0.121	2.02	0.019	460	0.73	0.02
	0.120	2.21	0.016	790	0.91	0.02
	0.120	2.21	0.016	1120	1.08	0.03
DC4	0.124	2.42	0.014	230	0.83	0.01
	0.123	2.42	0.013	460	1.19	0.01
	0.122	2.47	0.013	790	1.12	0.01
	0.122	2.47	0.013	1120	1.18	0.01
DC5	0.152	1.23	0.064	230	0.03	0.11
	0.152	1.23	0.064	460	0.02	0.28
	0.149	1.19	0.068	790	0.06	0.14
	0.146	1.19	0.066	1120	0.12	0.08
DC6	0.202	1.53	0.055	230	0.07	0.02
	0.202	1.53	0.055	460	0.04	0.11
	0.196	1.54	0.053	790	0.15	0.03
	0.195	1.56	0.051	1120	0.27	0.99
DC7	0.208	1.99	0.034	230	0.27	0.01
	0.208	1.99	0.034	460	0.28	0.01
	0.208	1.99	0.034	790	0.63	0.01
	0.199	1.99	0.032	1120	0.77	0.40

7. Conclusions

Dune protection interventions vary greatly in scale and complexity depending primarily on the extent of the existing dune system and on the degree of degradation that has affected the dune system. The effectiveness of the use of nanosilica was investigated with two physical models in the 2D wave flume of the EUMER laboratory at the University of Salento (Italy). The first part of the experimental campaign was carried out on a horizontal seabed to allow us to gain knowledge of the nanosilica properties related to hydrodynamic loadings and effective testing procedures. Compared with a natural loose sand bottom, the injection of colloidal nanosilica consolidated a surface layer of the seabed. The most interesting aspect concerning the first part of the experimental campaign is that the sediment mobility threshold of consolidated sand increased considerably. In the second part of the experimental study, the behavior of colloidal silica-based grout was investigated on a beach-dune system under irregular wave tests. Cross-shore profiles of a beach-dune system observed for seven different wave conditions in the case of natural sand and consolidated sand were compared. It was observed that, with the injection of the consolidating nanosilica-based grout, the cross-shore dune profile under five wave attacks remained practically unchanged; under the other two wave attacks, a delay in the erosion process was observed. The results demonstrate significant advantages in the use of nanosilica to improve erosion resistance of the dune.

From laboratory evidence, the use of nanosilica is found to be promising, although it should include a carefully planned procedure to achieve and maintain strong awareness and support within the broader community, as with any dune rehabilitation and management strategy. In this regard, research in several aspects can be further deepened,

such as the influence on aeolian transport, vegetation dynamics related to the deposition and erosion of the sediments at the dunes, and multi-scale consequences on biological components and the overall sediment balance in the coastal region. As already mentioned, several methods can be used to prevent dune erosion depending on the context and scale of degradation; they include the use of sand moving equipment or sand trapping techniques such as dune-forming fences, the spreading of brush matting, and revegetation. Comparing with more traditional solutions, the proposed intervention does not increase the dune size footprint, avoiding further obstacles. Moreover, it also has an economic implication since, paralleled with the cost of the material, which can vary depending on the context of the dune environment to be treated, there is a considerable saving on the costs of implementation of the intervention in terms of human resources and equipment to be used.

It is worth noting that several potential applications could be considered not only in the field of dune protection but also concerning phenomena in which hydrodynamic quantities such as turbulent and mean velocities, bed shear stress, and turbulent stresses undoubtedly govern the processes of entrainment, transport, and deposition [41,42].

A numerical model will need to be developed for practical applications of nanosilica grout and to investigate the behavior of consolidated sand on the beach-dune system across different time and space scales. The numerical model may be calibrated using the small-scale experiments in this study.

Author Contributions: Conceptualization and supervision of the investigation, N.K. and G.R.T.; laboratory investigation, E.L. and D.S.; data analysis and curation, writing—original draft preparation, E.L.; review and editing, A.F., S.D.B., and F.D. All authors have read and agreed to the published version of the manuscript.

Funding: This research was funded by the Regione Puglia through the grant project titled "Sperimentazione di tecnologie innovative per il consolidamento di dune costiere (INNO-DUNECOST)", POR Puglia FESR FSE 2014-2020-Sub-Azione 1.4.B, Contract n. RM5UKM2.

Institutional Review Board Statement: Not applicable.

Informed Consent Statement: Not applicable.

Data Availability Statement: Not applicable.

Acknowledgments: Authors thank the four anonymous reviewers for their fruitful comments.

Conflicts of Interest: The authors declare no conflict of interest.

References

1. Taveira-Pinto, F.; Rosa-Santos, P.; Fazeres-Ferradosa, T. Anthropogenic influences on Integrated Coastal Zone Management. *Rev. Gestão Costeira Integr.* **2020**, *20*, 215–217. [CrossRef]
2. Hamza, W.; Tomasicchio, G.R.; Ligorio, F.; Lusito, L.; Francone, A. A Nourishment Performance Index for Beach Erosion/Accretion at Saadiyat Island in Abu Dhabi. *J. Mar. Sci. Eng.* **2019**, *7*, 173. [CrossRef]
3. Gann, G.D.; McDonald, T.; Walder, B.; Aronson, J.; Nelson, C.R.; Jonson, J.; Hallett, J.G.; Eisenberg, C.; Guariguata, M.R.; Liu, J.; et al. International principles and standards for the practice of ecological restoration. Second edition. *Restor. Ecol.* **2019**, *27*, S1–S46. [CrossRef]
4. Gencarelli, R.; Johnson, B.; Kobayashi, N.; Tomasicchio, G.R. On dune erosion and breaching. In Proceedings of the 5th International Conference of Coastal Structures, Venice, Italy, 2–4 June 2007.
5. Gencarelli, R.; Tomasicchio, G.R.; D'Alessandro, F.; Frega, F. Dune erosion prediction during storm surges. In Proceedings of the International Conference on the Application of Physical Modelling to Port and Coastal Protection—Coastlab 08, Bari, Italy, 2–5 July 2008; Nuova Editoriale BIOS: Cosenza, Italy; pp. 113–116, ISBN 978-88-6093-046-0.
6. Martínez, M.L.; Hesp, P.A.; Gallego-Fernandez, J.B. *Coastal Dune Restoration: Trends and Perspectives*; Springer: Berlin/Heidelberg, Germany, 2013; pp. 323–339.
7. Gencarelli, R.; Tomasicchio, G.R.; Kobayashi, N.; Johnson, B. Effects of Hurricane Isabel along the North Carolina Coastline: Beach Profile Evolution and Dune Erosion. In Proceedings of the 3rd SCACR—International Short Conference on Applied Coastal Research, Lecce, Italy, 2–4 June 2008.
8. Fazeres-Ferradosa, T.; Welzel, M.; Schendel, A.; Baelus, L.; Santos, P.R.; Pinto, F.T. Extended characterization of damage in rubble mound scour protections. *Coast. Eng.* **2020**, *158*, 103671. [CrossRef]

9. Maza, M.; Lara, J.L.; Losada, I.J. Experimental analysis of wave attenuation and drag forces in a realistic fringe Rhizophora mangrove forest. *Adv. Water Resour.* **2019**, *131*, 103376. [CrossRef]
10. Kobayashi, N.; Gralher, C.; Do, K. Effects of Woody Plants on Dune Erosion and Overwash. *J. Waterw. Port Coastal Ocean Eng.* **2013**, *139*, 466–472. [CrossRef]
11. Kutiel, P.; Kutiel, H.; Lavee, H. Vegetation response to possible scenarios of rainfall variations along a Mediterranean–extreme arid climatic transect. *J. Arid. Environ.* **2000**, *44*, 277–290. [CrossRef]
12. Mason, T.; French, K.; Russell, K. Moderate impacts of plant invasion and management regimes in coastal hind dune seed banks. *Biol. Conserv.* **2007**, *134*, 428–439. [CrossRef]
13. Jonsson, I.G. Wave Boundary Layers and Friction Factors. *Coast. Eng.* **1967**, 127–148. [CrossRef]
14. Madsen, O.S.; Grant, W.D. Quantitative Description of Sediment Transport by Waves. *Coast. Eng.* **1977**, 1092–1112. [CrossRef]
15. Sleath, J.F. *Sea Bed Mechanics*; Ocean Engineering; Wiley: New York, NY, USA, 1984.
16. Nielsen, P. *Coastal Bottom Boundary Layers and Sediment Transport*; Tuh Tuck Link; World Scientific: Singapore, 1992; Volume 4.
17. Fredsøe, J.; Deigaard, R. *Mechanics of Coastal Sediment Transport*; World Scientific: Singapore, 1992; Volume 3, p. 369.
18. Van Rijn, L.C. *Principles of Sediment Transport in Rivers, Estuaries and Coastal Seas*; Aqua Publications: Amsterdam, The Netherlands, 1993; Volume 1006, pp. 11–13.
19. Soulsby, R.L. Dynamics of marine sands: A manual for practical applications. *Oceanogr. Lit. Rev.* **1997**, *9*, 947.
20. Nairn, R.B.; Southgate, H.N. Deterministic profile modelling of nearshore processes. Part 2. Sediment transport and beach profile development. *Coast. Eng.* **1993**, *19*, 57–96. [CrossRef]
21. Kobayashi, N.; Johnson, B.D.; Karjadi, E.A. Cross-Shore Sand Transport on Beaches. *Coast. Eng.* **2001**, 3165–3178. [CrossRef]
22. Dean, R.G.; Dalrymple, R.A. *Coastal Processes with Engineering Applications*; Cambridge University Press: Cambridge, UK, 2002.
23. Tomasicchio, G.R.; D'Alessandro, F.; Barbaro, G. Composite modelling for large-scale experiments on wave–dune interaction. *J. Hydraul. Res.* **2011**, *49*, 15–19. [CrossRef]
24. Tomasicchio, G.R.; Sánchez-Arcilla, A.; D'Alessandro, F.; Ilic, S.; James, M.R.; Sancho, F.; Fortes, C.J.; Schüttrumpf, H. Large-scale experiments on dune erosion processes. *J. Hydraul. Res.* **2011**, *49*, 20–30. [CrossRef]
25. D'Alessandro, F.; Tomasicchio, G.R. Wave–dune interaction and beach resilience in large-scale physical model tests. *Coast. Eng.* **2016**, *116*, 15–25. [CrossRef]
26. D'Alessandro, F.; Tomasicchio, G.R.; Musci, F.; Ricca, A. Dune erosion physical, analytical and numerical modelling. In Proceedings of the Coastal Engineering, Santander, Spain, 14 December 2012.
27. Sancho, F.; Abreu, T.; D'Alessandro, F.; Tomasicchio, G.R.; Silva, P.A. Surf hydrodynamics under collapsing coastal dunes. *J. Coast. Res.* **2011**, *64*, 144–148.
28. Brunone, B.; Tomasicchio, G. Wave Kinematics at Steep Slopes: Second-Order Model. *J. Waterw. Port Coast. Ocean Eng.* **1997**, *123*, 223–232. [CrossRef]
29. Paul, M.; Kamphuis, J.; Brebner, A. Similarity of Equilibrium Beach Profiles. *Coast. Eng.* **1972**, 1217–1236. [CrossRef]
30. Henry, P.Y.; Aberle, J. *Hydralab+ Deliverable D8.3 Protocols for Scaling Morphodynamics in Time*; Zendo: Genève, Switzerland, 2018.
31. Wallingford, H.R. Wave Gauge System: User Manual. Available online: http://equipit.hrwallingford.com/products/wave-gauges/wave-gauge-systems-8-channels (accessed on 10 September 2019).
32. Wallingford, H.R. 2D Bed Profiling System for Physical Models. Available online: https://www.hrwallingford.com/expertise/equipment-and-technology/instrumentation-and-software-physical-models (accessed on 10 September 2019).
33. Chieregato, A.; Salazar, C.G.O.; Todaro, C.; Martinelli, D.; Peila, D. *Test di Laboratorio di Iniezione per L'impermeabilizzazione e Consolidamento di Terreni Granulari per Mezzo di Materiali Innovativi*; GEAM (GEoingegneria Ambientale e Mineraria): Milan, Italy, 2014.
34. Mansard, E.; Funke, E. The Measurement of Incident and Reflected Spectra Using a Least Squares Method. *Coast. Eng.* **1980**, 154–172. [CrossRef]
35. Frostick, L.E.; McLelland, S.J.; Mercer, T.G. *Users Guide to Physical Modelling and Experimentation: Experience of the HY-DRALAB Network*; CRC Press: Boca Raton, FL, USA, 2011.
36. Mariotti, G.; Fagherazzi, S. Wind waves on a mudflat: The influence of fetch and depth on bed shear stresses. *Cont. Shelf Res.* **2013**, *60*, S99–S110. [CrossRef]
37. Zhu, Q.; van Prooijen, B.; Wang, Z.; Yang, S. Bed-level changes on intertidal wetland in response to waves and tides: A case study from the Yangtze River Delta. *Mar. Geol.* **2017**, *385*, 160–172. [CrossRef]
38. Shi, B.; Cooper, J.R.; Pratolongo, P.D.; Gao, S.; Bouma, T.J.; Li, G.; Li, C.; Yang, S.; Wang, Y.P. Erosion and Accretion on a Mudflat: The Importance of Very Shallow-Water Effects. *J. Geophys. Res. Oceans* **2017**, *122*, 9476–9499. [CrossRef]
39. Shields, A. Application of Similarity Principles and Turbulence Research to Bed-Load Movement. 1936. Available online: https://resolver.caltech.edu/CaltechKHR:HydroLabpub167 (accessed on 25 November 2019).
40. Van Gent, M.; Steetzel, H.; Boers, M.; Smith, J.M.; Coeveld, E.; Walstra, D.; Van De Graaff, J. Dune erosion tests to study the influence of wave periods. In Proceedings of the 30th ICCE, San Diego, CA, USA, 3–8 September 2006.
41. Zordan, J.; Juez, C.; Schleiss, A.J.; Franca, M.J. Entrainment, transport and deposition of sediment by saline gravity currents. *Adv. Water Resour.* **2018**, *115*, 17–32. [CrossRef]
42. Vahdati, V.J.; Yaghoubi, S.; Torabipour, A.; Correia, J.A.; Fazeres-Ferradosa, T.; Taveira-Pinto, F. Combined solutions to reduce scour around complex foundations: An experimental study. *Mar. Syst. Ocean Technol.* **2020**, *15*, 81–93. [CrossRef]